INTERNATIONAL JOURNAL FOR NUMERICAL METHODS IN FLUIDS
Int. J. Numer. Meth. Fluids **30**: 65–82 (1999)

ON NUMERICAL ERRORS AND TURBULENCE MODELING IN TIP VORTEX FLOW PREDICTION

JENNIFER DACLES-MARIANI[a,*], DOCHAN KWAK[b] AND GREGORY ZILLIAC[c]

[a] *Mechanical and Aeronautical Engineering Department, University of California, Davis, CA 95616, USA*
[b] *Advanced Computational Methods Branch, NASA Ames Research Center, Moffett Field, CA 94035, USA*
[c] *Fluid Mechanics Laboratory, NASA Ames Research Center, Moffett Field, CA 94035, USA*

SUMMARY

The accuracy of tip vortex flow prediction in the near-field region is investigated numerically by attempting to quantify the shortcomings of the turbulence models and the flow solver. In particular, some turbulence models can produce a 'numerical diffusion' that artificially smears the vortex core. Low-order finite differencing techniques of the convective and pressure terms of the Navier–Stokes equations and inadequate grid density and distribution can also produce the same adverse effect. The flow over a wing and the near-wake with the wind tunnel walls included was simulated using 2.5 million grid points. Two subset problems, one using a steady, three-dimensional analytical vortex, and the other, a vortex obtained from experiment and propagated downstream, were also devised in order to make the study of vortex preservation more tractable. The method of artificial compressibility is used to solve the steady, three-dimensional, incompressible Navier–Stokes equations. Two one-equation turbulence models (Baldwin–Barth and Spalart–Allmaras turbulence models), have been used with the production term modified to account for the stabilizing effect of the nearly solid body rotation in the vortex core. Finally, a comparison between the computed results and experiment is presented. Published in 1999 by John Wiley & Sons, Ltd.

KEY WORDS: incompressible flow; Navier–Stokes equations; tip vortex flow

1. INTRODUCTION

The study of wingtip vortices is of great significance in many areas of fluid engineering. Tip vortices generated by wings on a large aircraft have been known to affect other aircraft following at a close distance. The blade/vortex interaction on rotorcraft blades is another area of interest since this interaction can directly affect the rotorcraft performance and cause substantial vibration under some flight conditions [1]. On ship propeller blades, the tip vortex flow is of great concern in connection with cavitation inception and development studies [2]. Although there has been a great deal of work done on tip vortex prediction in the form of theoretical, experimental and computational studies, the current understanding of the intricacies of tip vortex flows is incomplete.

The flow field generated by a wingtip is often turbulent and highly three-dimensional, with existence of 'local separation' and secondary flows [3–5]. Thus, accurate prediction of the flow presents some challenges numerically and experimentally. Some attempts to further understand

* Correspondence to: NASA Ames Research Center, MS T27B-1, Moffett Field, CA 94035, USA.

Received 20 August 1997
Revised 13 May 1998

wake vortex flows and the implications for air traffic regulations were outlined and discussed in a paper by McCroskey [6]. This paper indicated that aerodynamics is not a fully mature technology. However, computational fluid dynamics at this stage can be used as a tool to complement experiments and flight tests in evaluating methods for wake vortex formation and roll-up. Recently, Dacles-Mariani *et al.* [7,8] computed a tip vortex flow on a rectangular wing with a rounded tip and compared the results side-by-side with experiment. A detailed study of current capabilities of existing numerical methods and one-equation turbulence models was initiated as part of this study [9,10]. The results of the earlier effort showed some success in capturing the flow features of the tip vortex in the near-wake region; however, the static pressure coefficient in the vortex core was not predicted well. This was improved, to some extent, in a subsequent computation [7].

Accurate computation of a tip vortex flow field requires resolution not only of the viscous boundary layer region, but also other areas with high flow gradients, such as in the vicinity of the vortex core and the near-field wake region. For these reasons, minimum numerical diffusion, sufficient grid density and appropriate distribution are essential. For the purposes of this study, the tip vortex flow has been categorized into three distinct stages: formation, growth and decay (see Figure 1). The first stage is the formation of the tip vortex on the suction side of the wing surface. Here, the pressure differences existing between the upper and lower side of the wing drives the boundary layer fluid to flow around the tip of the wing. In the second stage, the flow wraps up more and more of the boundary layer fluid, the tip vortex core begins to grow. The viscous core radius is defined as the distance between the point of minimum cross-flow velocity in the center of the vortex core to the point of maximum cross-flow velocity. During the growth stage, the vortex develops a very low pressure in the core, which in turn increases the axial velocity at the core. At some point after the trailing edge, the vortex begins to decay (third stage).

Inaccuracies in tip vortex flow prediction are generally manifested in three ways: (i) a free shear layer that is too thick and often with an incorrect angle of departure from the surface, (ii) a diffused or distorted core region, (iii) overprediction of static pressure coefficient at the core and correspondingly an underprediction of the peak axial velocity.

This paper is part of a comprehensive computational and experimental study to accurately compute the formation of a turbulent wingtip vortex [3–5,7–10]. In this paper, the numerical errors and numerical diffusion from turbulence models in tip vortex predictions are discussed. In order to make the problem more tractable, two subset problems were devised. A steady

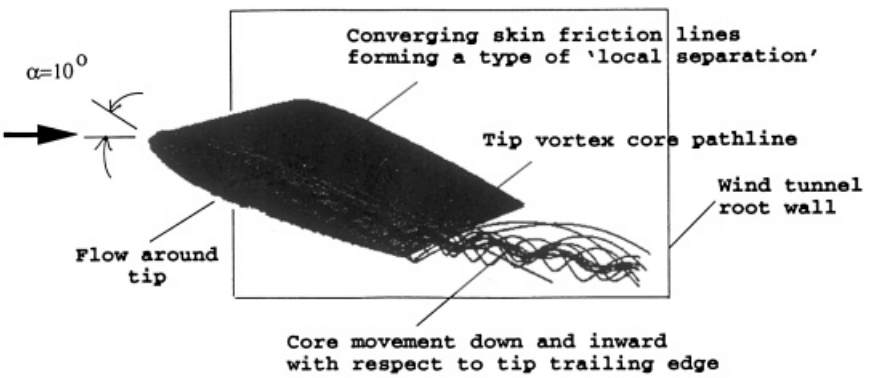

Figure 1. Tip vortex flow field with a rounded tip configuration.

three-dimensional analytical vortex was studied in detail to determine grid requirements to resolve the viscous core of the vortex. Also, the propagation of a vortex (obtained from experiment) in the wake region was analyzed. Findings on how grid refinement, the accuracy of the finite differencing of the convective terms, and the turbulence modeling affect the accuracy of the tip vortex flow are discussed and implemented on the full problem of flow over a rectangular wing with a rounded tip and angle of attack of 10°. The numerical approach section presents the governing equations and discusses the flow solver used for the study. The sources of numerical errors and shortcomings of the turbulence models are also outlined. Finally, comparisons with measured data are discussed.

2. NUMERICAL APPROACH

A three-dimensional, incompressible Navier–Stokes flow solver, INS3D-UP [11], was used in this study. The flow code uses an implicit finite difference scheme in generalized curvilinear co-ordinates written in a primitive variable formulation. The algorithm is based on the artificial compressibility method [12]. In this formulation, the continuity equation is augmented with a time derivative of pressure. The continuity equation is coupled with the momentum equations to form a hyperbolic system of equations, which are marched in pseudo-time to reach a steady state solution. The governing equations are:

$$\frac{\partial}{\partial \tau}\hat{D}+\frac{\partial}{\partial \xi}(\hat{E}-\hat{E}_v)+\frac{\partial}{\partial \eta}(\hat{F}-\hat{F}_v)+\frac{\partial}{\partial \zeta}(\hat{G}-\hat{G}_v)=R,$$

where R is defined as the residual vector and

$$\hat{D}=\frac{1}{J}\begin{bmatrix} p \\ u \\ v \\ w \end{bmatrix}, \qquad \hat{E}=\frac{1}{J}\begin{bmatrix} \beta U \\ \xi_x p+uU+\xi_t u \\ \xi_y p+vU+\xi_t v \\ \xi_z p+wU+\xi_t w \end{bmatrix},$$

$$\hat{F}=\frac{1}{J}\begin{bmatrix} \beta V \\ \eta_x p+uV+\eta_t u \\ \eta_y p+vV+\eta_t v \\ \eta_z p+wV+\eta_t w \end{bmatrix}, \qquad \hat{G}=\frac{1}{J}\begin{bmatrix} \beta W \\ \zeta_x p+uW+\zeta_t u \\ \zeta_y p+uW+\zeta_t v \\ \zeta_z p+uW+\zeta_t w \end{bmatrix},$$

$$\hat{E}_v=\begin{bmatrix} 0 \\ \hat{e}_v \end{bmatrix}, \qquad \hat{F}_v=\begin{bmatrix} 0 \\ \hat{f}_v \end{bmatrix}, \qquad \hat{G}_v=\begin{bmatrix} 0 \\ \hat{g}_v \end{bmatrix}.$$

Here, J is the Jacobian and the quantities U, V and W are contravariant velocity components and the metrics of the co-ordinate transformation are ξ_x, η_y, ζ_z. The viscous terms are represented as e_v, f_v and g_v.

The convective and pressure terms are evaluated using a fifth-order-accurate flux difference splitting based on Roe's method [13]. A second-order central difference scheme is used for the viscous terms. The resulting algebraic system of equations is then solved using a Gauss–Seidel line relaxation scheme.

2.1. Subset problem

Initial calculations indicated that an extremely fine mesh is required to resolve the tip vortex flow field. Consequently, in addition to a computation of a full problem, a subset problem (reduced computational domain) and an analytical vortex flow were studied. This enabled grid refinement and turbulence model testing to be more tractable.

2.1.1. Analytical vortex study. The analytical, self similar free vortex solution of Rott [14] was investigated in detail to perform grid resolution and refinement study. This vortex is an exact solution to the Navier–Stokes equation. It is a steady, three-dimensional axisymmetric vortex given by:

$$v_r = -ar,$$

$$v_\theta = \frac{\Gamma_\infty}{(2\pi r)}(1 - e^{-ar^2/2\nu}),$$

$$v_x = 2ax.$$

In the first equation, v_r is the velocity in the radial direction with a as the velocity gradient and r as the radius. In the second equation, Γ_∞ is the vortex circulation in the free-stream and ν is the kinematic viscosity. Finally, in the third equation v_x is the velocity in the streamwise direction. To start the computation, the vortex is located on the centerline of the domain and extended downstream for about three core radii. The far-field boundaries range from $-4.35r_c$ to $4.35r_c$ in the vertical and horizontal direction (with r_c the core radius in the inflow). This relatively small domain was chosen since it is similar in size to that of the wake case. The inflow, outflow and side boundary conditions were determined from the analytical solution.

2.1.2. Wake case study. The computational domain for this vortex preservation test includes the region from the trailing edge of the full problem to 0.69 of the chord length c, downstream of the trailing edge. The experimentally measured velocity profile in a plane of the trailing edge of the wing is imposed at the inflow, while the inflow boundary condition for the pressure is computed based on the method of characteristics using the one-dimensional Riemann invariants. The exit conditions are satisfied by prescribing an experimentally determined pressure distribution. The velocity components at the outflow are calculated by using one-dimensional Riemann invariants.

2.2. Full problem

The computational domain consists of the wing wind tunnel wall and the near-wake geometry, as shown in Figure 2, which is a close approximation to the 32 in. $\times$ 48 in. low speed wind tunnel and wing set-up at the Fluid Mechanics Laboratory, NASA Ames Research Center [8–10]. The computational domain includes a rectangular half-wing with a NACA 0012 airfoil section, a rounded wing tip and the surrounding boundaries. The wing has an aspect ratio of 0.75 and was mounted inside a wind tunnel at an angle of attack of 10°. The flow is turbulent with a Reynolds number of 4.6 million based on the chord length.

The inflow velocity boundary condition was prescribed using measured values from experiment while the inflow pressure was computed based on the method of characteristics using one-dimensional Riemann invariants. At the solid surface (wind tunnel walls and the surface of the model), the velocity was specified to be zero. At the outflow, the pressure was prescribed using the measured values, but the velocity distribution was computed based on the method of characteristics.

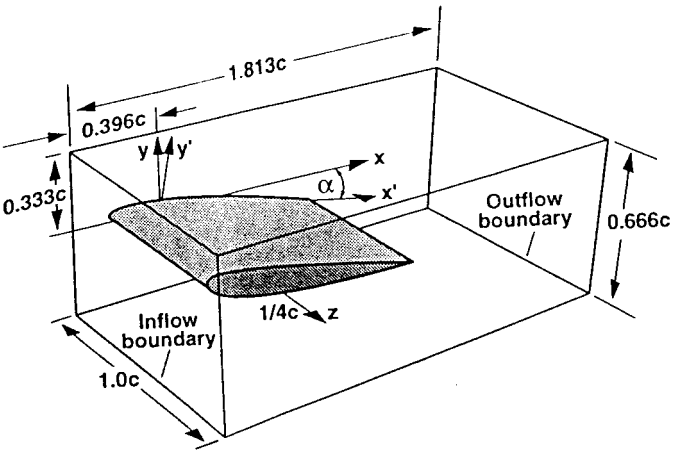

Figure 2. Computed and measured domain.

Because of the close proximity of the wind tunnel walls and corner regions to the wing surface, the grid generation process was not straightforward. A single zone grid of C–O topology was used for the complete geometry. The grid was a hybrid grid consisting of an inner hyperbolic grid (generated using HYPGEN [15]) surrounding the wing, matched with an elliptic grid (generated using GRIDGEN2D [16]) near the wind tunnel walls to form the base grid. The three-dimensional volume grid was then generated by stacking the two-dimensional grid along the straight section of the wing and wrapping the grid around the rounded wing tip. The wrapping procedure was done in such a way as to avoid the interpolation of values where the tip vortex is forming. The volume grid was made to conform to the wind tunnel wall geometry. One area of uncertainty is the wake cut topology. Typical of a C-type grid is the necessity of prescribing how the wake cut should behave in the wake region. To minimize grid-related errors, a trial and error grid generation procedure was performed to determine a wake cut position that does not interfere with the vortex core trajectory.

3. NUMERICAL ERRORS AND NUMERICAL DIFFUSION FROM TURBULENCE MODELS

Sources of numerical errors considered in this study are attributed to grid effects and accuracy of the differencing technique of the convective terms (i.e. truncation error of the discrete equation that is larger than the physical diffusion) encountered from the analysis of the analytical vortex study and the wake case vortex propagation. In this section, findings from these subset problems are applied to the full geometry.

3.1. Grid effects

Some of the grid-related errors come from skewness of grid lines and grid points that are not properly distributed. Improper distribution of the grid points can result in underresolving (i.e. artificially diffusing) the high gradients in the flow. If numerical diffusion arising from the grid-related errors and truncation errors exceed that of the physical diffusion, the computed vortex will be distorted.

For the full problem, the coarsest grid size was 0.6 million grid points ($83 \times 103 \times 53$). The viscous grid spacing was $1 \times 10^{-4}c$ on the wing surface, and $1 \times 10^{-3}c$ on the root wall and wind tunnel walls. The number of grid points across the viscous vortex core was less than 10 points. (No special attention was given to refining the grid in the vortex core region.) The next finer grid size consisted of 1.1 million grid points ($103 \times 145 \times 73$). Viscous grid spacings of $1 \times 10^{-5}c$ on the wing surface and $1 \times 10^{-4}c$ on the wind tunnel walls were used. Here, 15–20 grid points were concentrated across the viscous vortex core. The third grid consists of 1.5 million grid points ($115 \times 157 \times 83$). The viscous grid spacing on the wing was done differently; a viscous grid spacing of $1 \times 10^{-6}c$ was used on the wing surface, but this spacing was linearly expanded to $1 \times 10^{-5}c$ at the trailing edge and to $1 \times 10^{-3}c$ at the outflow wake line. This procedure helped redistribute points away from the wake cut in the wake region to locations close to the vortex. On the root wall and wind tunnel walls, a viscous grid spacing of $1 \times 10^{-4}c$ was specified. A grid size requirement of 15–20 grid points across the core was enforced in an attempt to resolve the core. Lastly, a grid consisting of 2.5 million grid points ($115 \times 189 \times 115$) was generated. This grid is similar in distribution to the 1.5 million grid but in the cross-flow plane in the vicinity of the viscous vortex core, the grid was refined by increasing the number of grid points across the vortex core to 22–30 grid points. Significant grid generation improvements were incorporated in the last two grid sizes, including redefining the wake cut topology and 'hand-adaptive' clustering of grid points in the vortex core.

3.2. Convective term discretization effects

Another source of artificial spreading of the vortex, arising from numerical diffusion, can be attributed to the differencing order of the convective and pressure terms. Higher-order-accurate differencing schemes have been shown to reduce numerical diffusion errors considerably in inviscid vortex preservation tests [17]. Early calculations [3] showed that a third-order-accurate scheme is too diffusive. This was evident from a grid refinement study of the subset problems, which are discussed in the Section 4. The results from an earlier paper [4] show that using a fifth-order differencing scheme causes a reduction of the numerical diffusion caused by the truncation error of the convective terms. In the current application, an upwind-biased fifth-order-accurate method developed by Rais [17] implemented in the discretization of the convective terms.

3.3. Turbulence modeling

Turbulence models can also be numerically diffusive. Here the issue is attributed to a more fundamental problem, being that the eddy viscosity approach is inappropriate in several ways for tip vortex flows. However, since the eddy viscosity model is being used in most aerodynamic flow simulations, this model is used in the present study. One source of error in this approach is the treatment of the production of turbulence typical of one-equation turbulence models. Some production term formulations have the effect of increasing the eddy viscosity in the core region where, in fact, the eddy viscosity should be very low. The effect of these errors on the computed vortex is similar to that of the numerical errors.

Measured results [9] indicate that the Reynolds stress and the mean strain rate are not aligned. This important finding implies that an eddy viscosity approach (constant or isotropic) will most likely not be fully successful. Since a full Reynolds stress model is not a realizable option at this point, two one-equation models often used in aerodynamic calculations were selected for this study; they are the Baldwin–Barth (BB) turbulence model [18] and the Spalart–Allmaras (SA) turbulence model [19].

Preliminary computations indicate that these models, though successful in predicting the overall flow pattern, both overpredict the level of eddy viscosity in the vortex core. This shortcoming can be overcome by modification of the production term, suggested by Spalart [20], and implemented in both of these models [3,4]. The production term P is approximated by

$$P = C_l \bar{\nu} S.$$

For the Baldwin–Barth model, C_l is a constant, $\bar{\nu}$ is the working variable νR_τ, where ν is the laminar viscosity and R_τ is the turbulent viscosity and S is a scalar measure of the deformation tensor. In the Spalart–Allmaras model, C_l is a constant (different from the Baldwin–Barth model), $\bar{\nu}$ is the working variable, and S is a scalar measure of the deformation tensor. The modification is implemented such that a combination of basing S on the magnitude of vorticity $|\omega|$ and on the strain rate $|s|$ is used giving:

$$P = C_l \bar{\nu}(|\omega| + 2 \min(0, |s| - |\omega|)).$$

Note that the factor 2 in this equation is an arbitrary constant that can be adjusted depending on the amount of numerical diffusion the turbulence model gives. This modification represents an attempt to empirically adjust the production term for vortex dominated flows, which are unusual flows in that there are regions that have high vorticity and low strain. The advantage of the formulation (shown in [5]) is that the eddy viscosity is reduced in the regions where the vorticity exceeds the strain rate, such as in the vortex core where the pure rotation should suppress the production of turbulence. The modification is not present in the shear layers; therefore, it does not interfere with the validation process.

The effects of the one-equation models with and without the modification of the production term, and the effect of improving the order of accuracy on the finite differencing technique, are discussed in the Section 4. (A detailed comparison is given in [4].) The turbulence model modification has the greatest effect on the axial velocity at the core center, but this modification alone is not sufficient. This represents a substantial improvement at little cost because the additional terms were added explicitly to the right-hand-side of the finite difference Navier–Stokes equations (banded matrix remained the same size).

4. RESULTS

A substantial amount of measured and computed results have been acquired during the course of this study. For further information, the reader is encouraged to refer to previously published papers

4.1. Subset problem

4.1.1. Analytical vortex study. Proper grid resolution of the vortex core is important in computing the correct growth rate of a vortex. Unfortunately, limited computational resources make the performance of a comprehensive grid refinement study of the full problem unachievable at this time.

In the current study, grid refinement tests were performed on a subset problem derived by Rott as the basis of comparison [4]. Since Rott's analytical solution is for an isolated free vortex (no wing), the approach taken was to find an effective Reynolds number that would produce a similar inflow velocity profile (and hence similar circulation level) to that of the

experiment. In order to isolate the effect or grid refinement alone, the code was run laminar using this effective Reynolds number. The solutions were obtained using fifth-order-accurate upwind-biased differencing of the convective terms for four grids of size 7056 ($16 \times 21 \times 21$), 26896 ($16 \times 41 \times 41$), 59536 ($16 \times 61 \times 61$) and 104976 ($16 \times 81 \times 81$) points and of uniform grid spacing.

Presented in Figure 3(a) and (b) are the peak core velocity magnitude and the cross-flow velocity magnitude ($\sqrt{v^2 + w^2}$) respectively (note, $r_c \approx 0.035c$ of the full geometry problem). As can be seen from these figures, grid independence was achieved for the two finer grids (in Figure 3 $\Delta y1'$, refers to the 7056 point grid, etc.). The grid refinement study shows that an average of 15–20 grid points (in each of the crosswise and spanwise directions) in the viscous core region are needed to adequately resolve the flow. It was also determined that the vortex is more sensitive to cross-flow plane grid refinement than streamwise refinement.

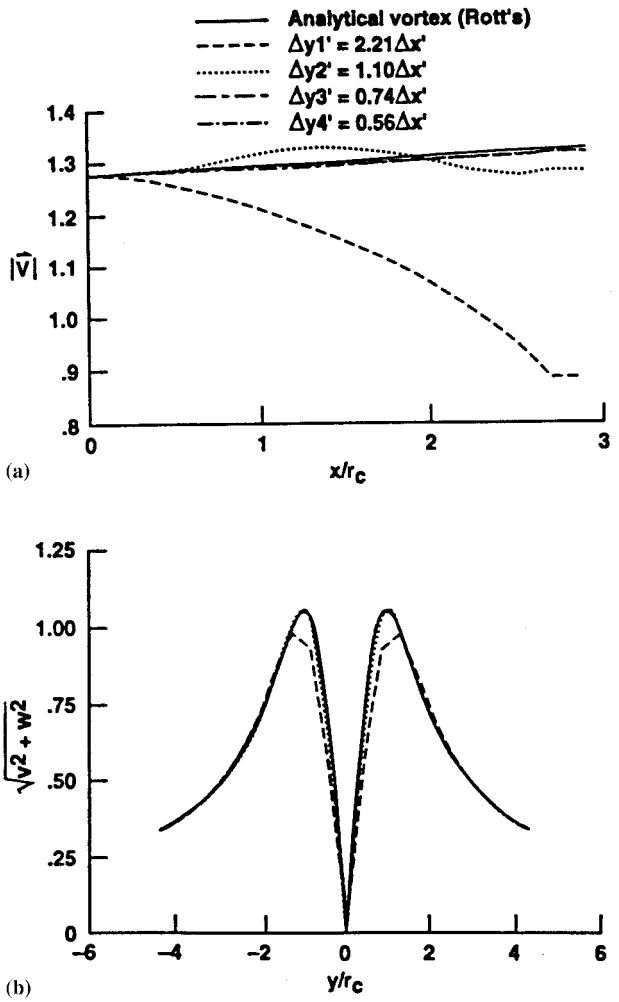

Figure 3. Analytical vortex propagation study [4]. (a) Peak velocity magnitude at the core; (b) cross-flow velocity magnitude across vortex core.

4.1.2. Wake case study. In addition to the grid refinement studies performed using Rott's vortex, a second approach taken to isolate the grid effects was to turn the turbulence model off while leaving the molecular viscosity on. Grid refinement was then performed for this case. Note that since measured inflow boundary conditions were used, these laminar computations were still a reasonable model problem of the vortex generated by the complete configuration (for studies of grid refinement, grid distribution and other numerical issues). Finally, wake case solutions were obtained using the Baldwin–Barth turbulence model implemented with two variations of the approximation of the production term [4].

Early on in this study, it was found that the third-order-accurate differencing scheme for the convective terms of the momentum equations was too diffusive for the flow conditions specified. Presented in Figure 4(a) and (b) are comparisons of third-order- and fifth-order-accurate differencing of the solution for a wake case grid having 371 000 points ($35 \times 103 \times 103$). Note the high level of velocity at the core. This velocity excess is a characteristic of strong vortices in their early stages of development as explained in [9]. In Figure 4(b) the core center velocity is underpredicted by roughly 25% for the cases with no turbulence model modification. In fact, for these cases, the velocity at the center of the core is less than that found in the outer portion of the core.

4.2. Turbulence modeling for the wake case study

Preliminary results from the Baldwin–Barth one-equation model and the Spalart–Allmaras one-equation model showed that in their original formulation, they both diffuse the vortex viscous core in a similar manner. Figure 4(c) illustrates the effect that the Baldwin–Barth turbulence model modification has on the eddy viscosity found in the vortex core. Notice how the results for the unmodified Baldwin–Barth model show a high level of eddy viscosity at the vortex core center, which was contrary to what was observed in the experiment, indicating that the unmodified model was too diffusive in the vortex core and is what prompted the turbulence model modification. The Spalart–Allmaras model behaved similarly when the modification was used. A detailed comparison between the two models will be presented in the full geometry discussion. The improvements obtained by these modifications are very significant, but the results are still not completely free of error (caused by the numerics and the model), at the center of the vortex core.

4.3. Full geometry

The single grid approach to this study was beneficial from the standpoint of error source identification. A total run time of 28 CPU hours on the Cray C-90 was required for the 2.5 million grid points case to obtain a fifth-order of magnitude drop of the residual. It should be noted that this study focuses primarily on resolving the fundamental issues involved in tip vortex computations without addressing the need to reduce the total number of grid points. However, it is recognized that for more practical implementations, the grid density requirement will have to be further addressed.

In the vortex formation stage, the numerical error was reduced by refining the grid in the turbulent boundary layer and also in the departing free-shear layer from the wing. As the vortex grows, the angle of departure of the boundary layer fluid from the surface was consistent with experimental results. However, the effect of the turbulence model is not known. The propagation of the vortex in the wake region proved to be successful. The high gradients of the cross-flow velocity compared well with experiment as well as the size of the

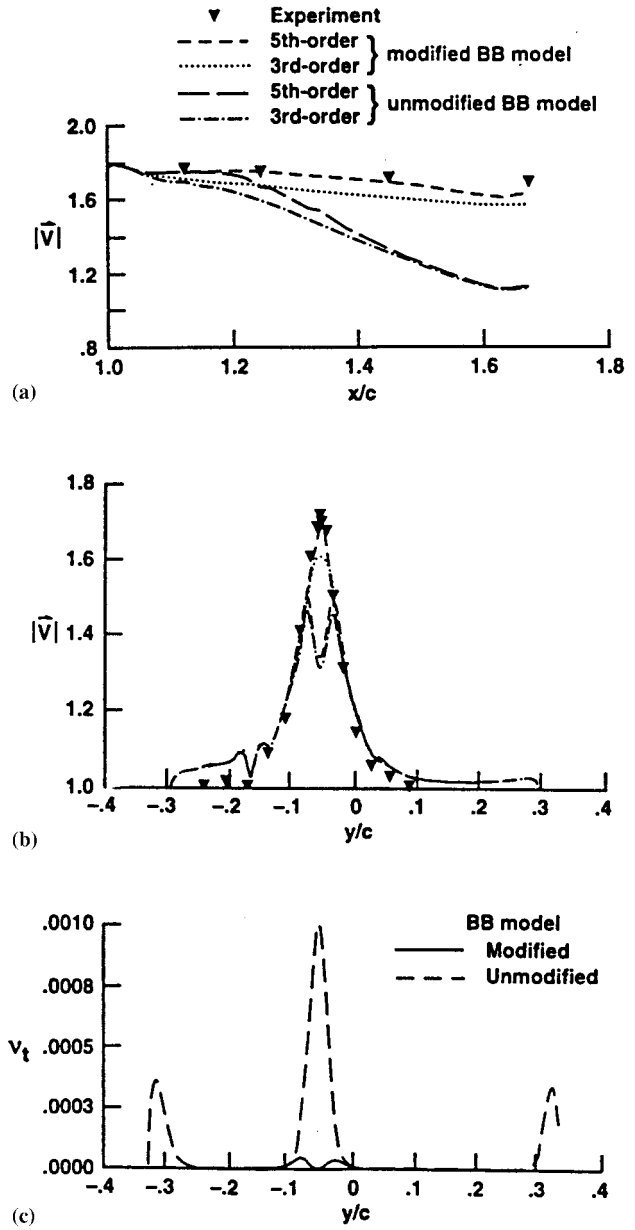

Figure 4. Wake case vortex propagation study [4]. (a) Peak velocity magnitude at vortex core; (b) total velocity magnitude across vortex core at $x/c = 1.241$; (c) eddy viscosity profile across vortex core at $x/c = 1.241$.

viscous core. The numerical diffusion was minimized as will be discussed later, and the extra numerical diffusion introduced by the turbulence models was also minimized, but is still an ongoing problem.

4.4. Numerical errors owing to grid density/distribution

Presented in Table I are some results and observations from the grid refinement study at $x/c = 1.241$ in the wake region downstream of the trailing edge. The maximum difference between experiment and computation is found in the core centerline values tabulated here. For the 1.5 million grid size, it is possible to obtain a reasonable prediction of the core axial velocity, yet significantly underpredicts the magnitude of the static pressure. The static pressure coefficient shows the poorest comparison of the quantities studied.

For the coarse grid computations (less than 1.5 million), it was not clear as to what extent numerical errors and 'errors' from turbulence models contribute to the artificial spreading of the vortex. This is because these effects are manifested in similar ways, i.e. the vortex is diffused faster compared with experiment. The authors found from previous analyses [3–5] that the first and foremost requirement to reduce the numerical diffusion was to modify the turbulence model production terms such that the eddy viscosity at the vortex core is a minimum instead of a maximum value. The improvement of the core axial velocity and static pressure comparisons was readily apparent (i.e an excess core axial velocity is obtained, as opposed to a deficit [4]). To further reduce the numerical diffusion, one can implement a higher-order differencing technique or increase the number of grid point requirements. Since the use of the fifth-order scheme does not increase the CPU requirement much, and since it is desired to use the minimum number of grid points required for an accurate solution, the case of higher-order differencing was preferred over increasing the number of grid points in the core. For the grid size of 1.5 million grid points, it was found that the two errors are equally important; the numerical error was of the same order of magnitude or less than turbulence modeling 'error' in the wake region.

To determine if numerical error was still present for this case, further grid refinement was performed and a 2.5 million grid point case was completed using the SA model. The Spalart–Allmaras model was chosen for the fine grid calculation because it showed detailed resolution of the vortex formation on the wing that was not seen in the Baldwin–Barth model. When the cross-flow plane was refined one and one-half times, the grid size in the core vicinity,

Table I. Effect of grid refinement and turbulence models ($x/c = 1.241$)

Grid size (million)	$\lvert V\rvert$ at vortex core centerline	Maximum cross-flow velocity near core	C_p minimum static at core centerline	Comments
0.6 (BB model)	1.03	0.55	−0.60	Vortex highly diffused with no peak velocity seen
1.1 (BB model)	1.31	0.91	−1.32	Peak velocity not clearly observed
1.5 (BB model)	1.72	0.980	−2.73	BL resolved, wake topology modified, grid improved. Peak velocity resolved well, vortex symmetric in shape
1.5 (SA model)	1.70	1.06	−2.77	Similar behavior as BB but more detailed features of the vortex are observed (e.g. detailed account of the wrapping around of fluid)
2.5 (SA model)	1.799	1.02	−3.10	Cross-flow plane refine 1.5× previous grid
Experiment	1.75	0.93	−3.51	

improvement in the comparison of the core properties are observed. In Figure 3(a) and (b) the cross-flow velocity profile and static pressure coefficient profiles are shown for different stations in the wake region. The dependent quantities have been circumferentially averaged in order to present the three-dimensional data in a form that allows for easy comparison. Here, the size of the vortex core seems to be maintained as it convects downstream demonstrating the fact that numerical diffusion is small.

A fine grid calculation of 2.5 million grid points compared with the coarser grid results, showed that complete grid independence was not reached. However, some improvement in the viscous core region was observed. The vortex propagated in the wake region with minimum numerical diffusion. Figure 4(a) and (b) compare the effective cross-flow velocity profiles and static pressure respectively, for the grids considered. Note here that some amount of numerical diffusion is still present for the 1.5 million grid points as shown by the slightly diffused static pressure profile inside and immediately outside of the vortex core. For the grid size of 2.5 million, excellent agreement of the flow gradients are found except close to the center of the vortex core. Notice also the improvement in the prediction of the core radius (Figure 4(a)) for the finer grid. The static pressure coefficient is still not well-predicted in Figure 4(b), but a noticeable improvement in the viscous core velocity distribution (Figure 4(b)) was achieved, although there are still discrepancies between experiment and computation. A possible explanation is that the turbulence model is causing the discrepancy in core static pressure as will be considered in the next section.

4.5. Turbulence model effect on core static pressure

Phillips and Graham [21] have performed a balance of terms in the mean momentum equations for the case of a turbulent trailing vortex. They considered the mean momentum equations for steady axisymmetric flow in cylindrical co-ordinates (r, θ, z) with the corresponding mean velocity components(v_r, v_θ, v_z). The r-momentum equation without approximation is:

$$\frac{\partial}{\partial z}(v_r v_\theta + \overline{v'_r v'_z}) = -\frac{\partial p}{\partial r} + \frac{1}{Re}\left\{\frac{\partial}{\partial r}\left(\frac{1}{r}\frac{\partial}{\partial r}(r v_r)\right) + \frac{\partial^2 v_r}{\partial z^2}\right\} - \frac{1}{r}\frac{\partial}{\partial r}(r v^2 + r\overline{v'^2_r}) + \frac{1}{r}(v_\theta^2 + \overline{v'^2_\theta}).$$

The boundary layer-type of assumption, which is applicable to a trailing vortex, is imposed (i.e. $\partial/\partial z \ll \partial/\partial r$ and $v_r \ll v_\theta$). In this study, this assumption only applies to the vortex in the wake region and not when it is forming on the wing surface. It has been shown that for a turbulent vortex, assuming that $\overline{v'^2_\theta} = \overline{v'^2_r}$ (where $\overline{v'^2_\theta}$ is the turbulent normal stress in the circumferential and $\overline{v'^2_r}$ is the turbulent normal stress in the radial direction) one gets

$$\frac{\partial p}{\partial r} = \frac{v_\theta^2}{r} - \frac{\partial}{\partial r}\overline{v'^2_r}.$$

As the flow progresses downstream (above the wing surface), the maximum circumferential velocity v_θ increases in the vortex core. In turn, an axial pressure gradient develops that greatly lowers the core static pressure. Consequently, the core axial velocity starts to increase. The dominant term that contributes to the radial pressure gradient, $\partial p/\partial r$, in a vortex is the term which contains v_θ. Note, however, that the second term on the right-hand-side of the equation may not be neglected because of the high near-field core turbulence intensities measured in the experiment [7]. This shows that the resolution of the core properties are dependent not only on the circumferential velocity, but also on the turbulent stress terms. If this term is not properly accounted for (which, as discussed previously, is not properly modeled by the one-equation turbulence models in vortex flows), a very good comparison between measured and computed values may not be achieved.

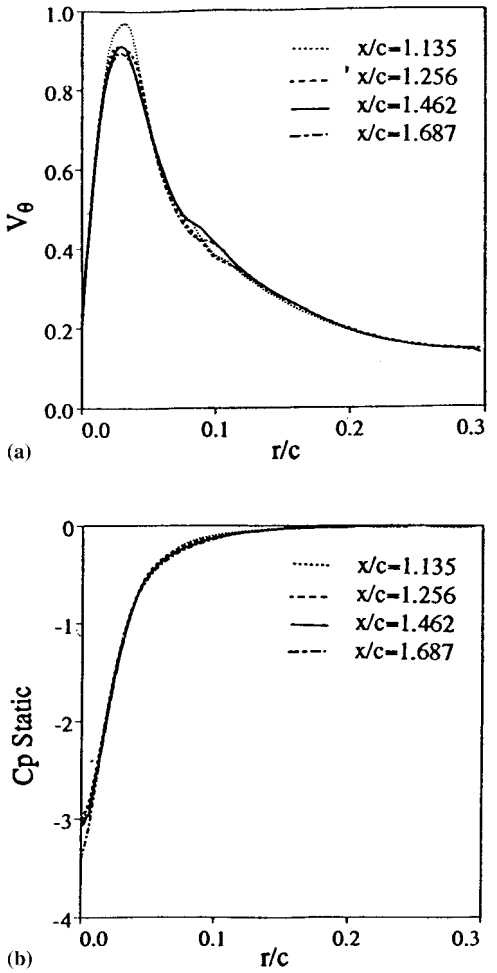

Figure 5. Vortex propagation in the wake region (2.5 million grid points). (a) Effective cross-flow velocity profile; (b) static pressure coefficient profile.

Further detailed differences can be seen by plotting the cross-flow velocity contours. Above the wing surface (Figure 5), a region of high and low cross-flow velocity (shown as red to blue contours respectively) whipping around the wing is observed. The computation using 1.5 million grid points and the BB model shows an overall distribution similar to that of the experiment, with the exception of the low cross-flow velocity region shown in blue contours. Here, the details of the smaller recirculation observed in the experiment was not captured in this computation. The next computation uses the same grid but this time the turbulence model was changed to the SA model. Notice that this gave a trend similar to the previous run with the BB model. The difference is observed in the low cross-flow velocity region on the wing surface. Here the SA model resolves this region showing the detailed recirculation inside but is still not similar to the experiment. Refining the grid further to 2.5 million grid points enhanced the contours levels but no further improvement is observed in the low cross-flow velocity area. Also, the 1.5 million grid point calculations produced some 'jaggedness' on the free shear layer profile coming off from the suction side of the wing for both models. When the grid was refined to 2.5 million, a smoother profile was obtained.

Further downstream at the outflow plane, Figure 6, the overall features between the computations are very similar. Most of the differences, however, can be seen in the resolution of the viscous vortex core. An elliptic core region is observed using a 1.5 million grid point and the BB model. Some (but not all) of the elliptic nature has been eliminated using the SA model. Finally, by refining the grid to 2.5 million and still using the SA model, all of the artificial elliptic behavior in the core has been eliminated (see Plates 1 and 2).

Although subtle differences are observed in some very specific regions of the tip vortex development using the BB and SA models, these differences seem to be localized and do not dramatically affect the overall features of the vortex. This was observed by performing some detailed comparison of the peak velocity and pressure profiles in the viscous vortex core region, and the location of the vortex as a function of streamwise distance.

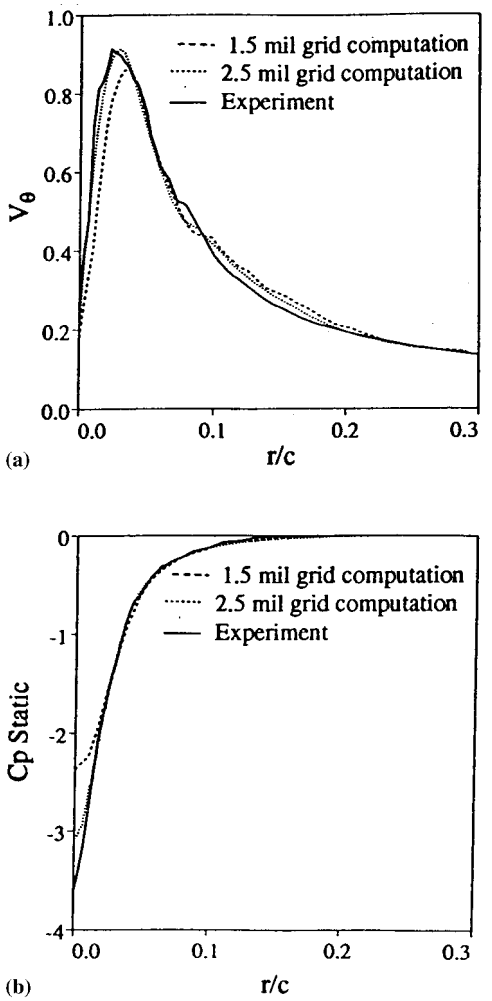

Figure 6. Comparison of flow quantities in the wake region at $x/c = 1.462$ for two grid sizes. (a) Effective cross-flow velocity profile; (b) static pressure coefficient profile.

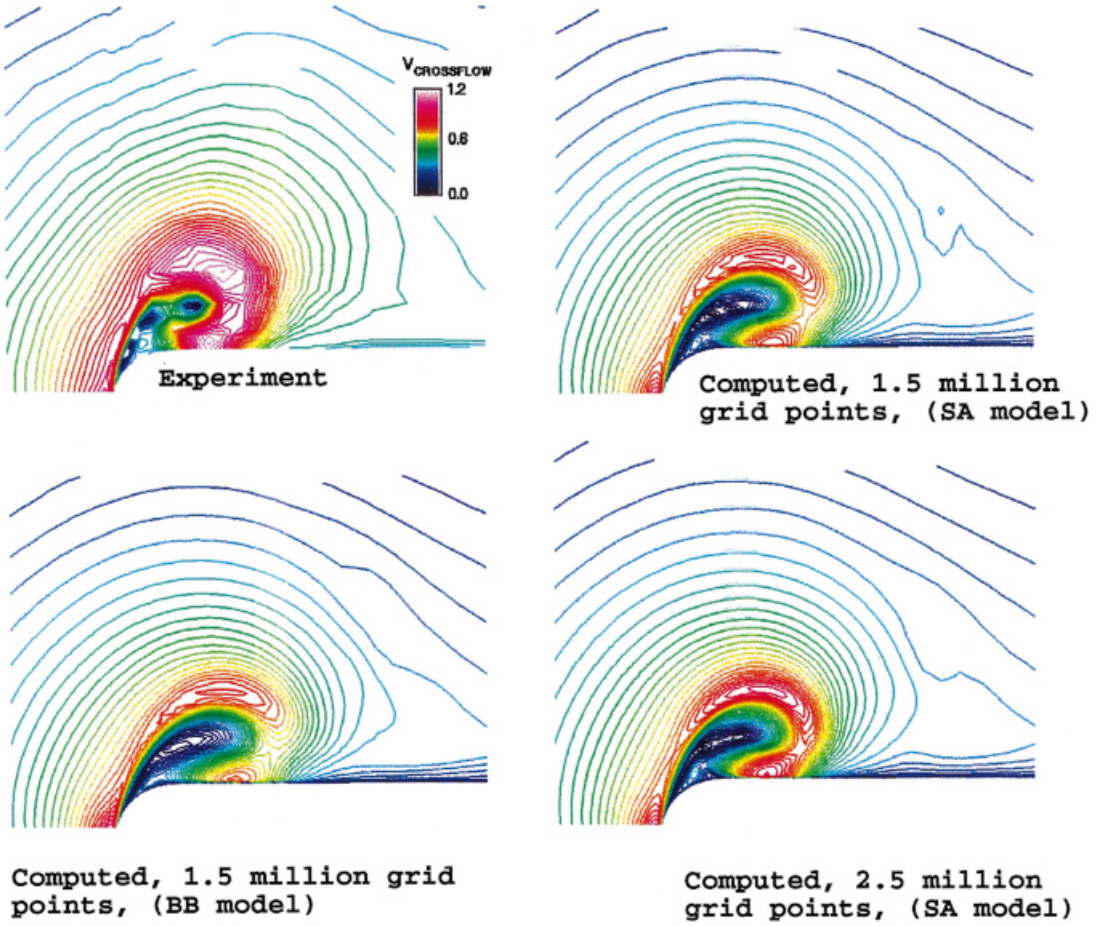

Plate 1. Comparison of cross-flow velocity contours at $x/c = 0.813$ using the BB model and the SA model. Also shown is the effect of refining the grid on the SA model.

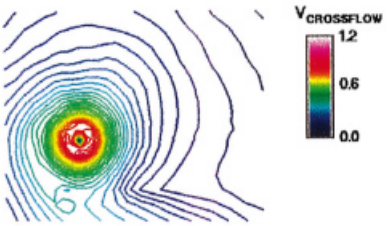

Experiment

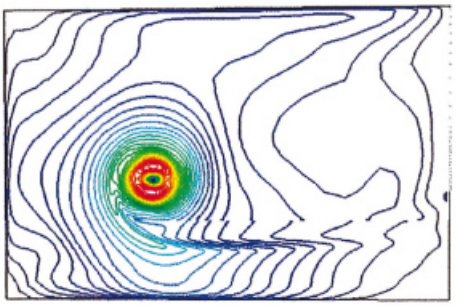

Computed, 1.5million grid points, (SA model)

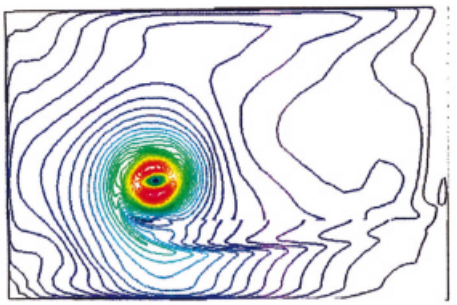

Computed, 1.5 million grid points, (BB model)

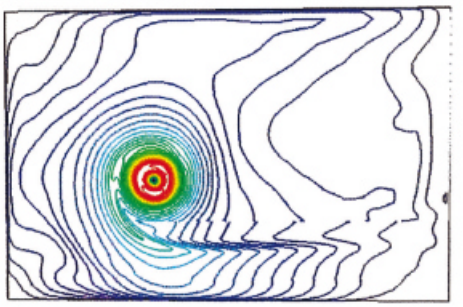

Computed, 2.5 million grid points, (SA model)

Plate 2. Comparison of cross-flow velocity contours at $x/c = 1.687$ using the BB model and the SA model. Notice that an elliptical-shaped vortex is computed using the 1.5 million grid points for both models. However, when the grid is refined, this behavior goes away.

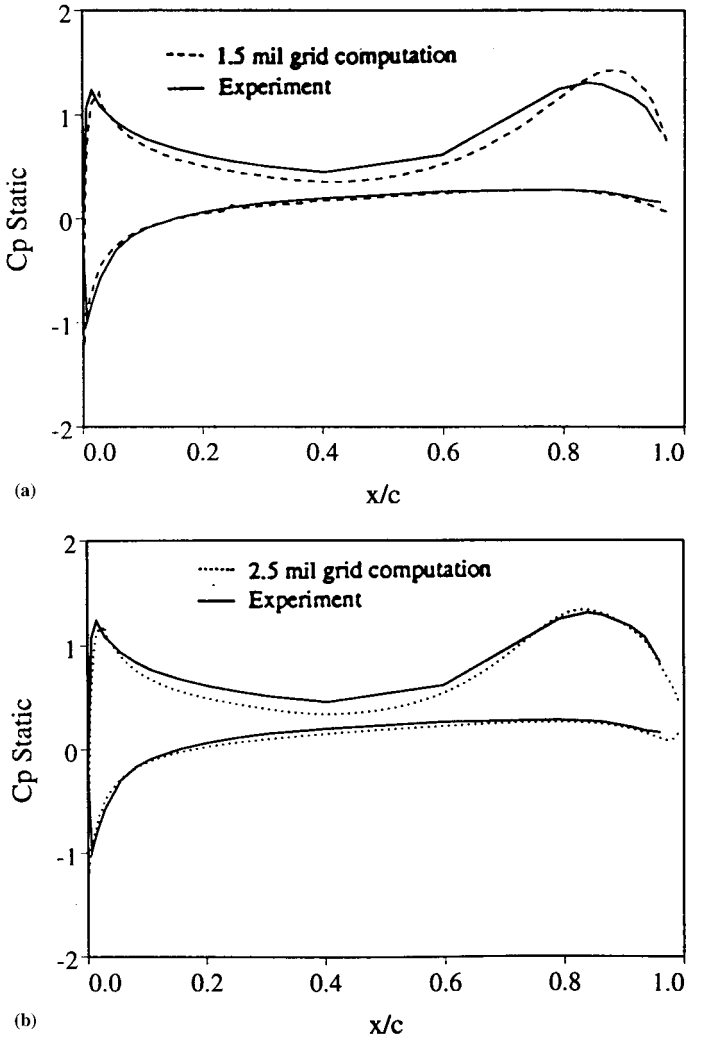

Figure 7. Comparison of surface static pressure at $z/c = 0.667$. (a) Computation using 1.5 million grid points; (b) computation using 2.5 million grid points.

In previous computational studies, the magnitude and extent of the surface pressure contour on the wing surface have been underpredicted. Of particular interest in this region is the pressure peak induced by the presence of the vortex above the suction side of the wing. Shown in Figure 7 are comparisons of a chordwise static pressure coefficient plot between experiment and the computational results using 1.5 million grid points (Figure 7(a)) and the computational results using 2.5 million grid points (Figure 7(b)). The general trends and the pressure levels of the computed and measured results agree well. Some differences though can be seen around the vortex-induced peak region for the 1.5 million grid point result. When the grid was selectively refined to 2.5 million grid points, a better agreement between computated and measured data was observed.

Table II. Tabulated values of computed lift and drag coefficients

Grid size (million)	C_D	C_L
2.5 ($115 \times 189 \times 115$)	0.1624	0.512
1.5 ($115 \times 157 \times 83$)	0.1620	0.513
1.1 ($103 \times 145 \times 73$)	0.1448	0.435
0.6 ($83 \times 130 \times 53$)	0.1267	0.405
Experiment	—	0.51

4.6. Effect on lift and drag coefficient

Ultimately, the goal of a detailed study such as this is to improve the design of aircraft, i.e. better prediction of lift and drag. Table II presents the lift and drag coefficient for the four grid sizes. Here, the grid sizes ranging from 0.6 million to 1.5 million are run using the BB model while the 2.5 million grid used the SA model. Since the grid refinement procedure was not systematic, the prediction of C_D and C_L for the two coarse grid sizes (0.5 million, 1.1 million) was very different from the two finer grids (1.5 million, 2.5 million). The two coarser grids did not take into account the modification of the turbulence model. In addition, the grid distribution in the boundary layer was not fine enough to capture the high flow gradients. In contrast, the two finer grids have the improvements mentioned in this paper. The two grids are very similar to each other except that the 2.5 million grid has 1.5 times as many grid points in the vortex core vicinity. Table II shows that although grid independence is not yet reached with the finest grid, the lift and drag coefficients do not change that much between the two fine grids ($< 0.2\%$). However, the difference between the measured values and the 2.5 million grid calculation is 0.39%. The measured C_L, values were obtained by integration of the C_p distribution and are not considered to be very accurate owing to insufficient number of points (pressure taps) used in the integration process.

5. CONCLUDING REMARKS

This study attempted to quantify to what extent numerics and turbulence models affect the accuracy of tip vortex flow prediction in the formation, growth and decay stages. In order to make this complex problem more trackable, two subset problems were considered: the analytical vortex due to Rott and the wake case propagation problem.

Some important findings stemming from these subset problems include using the fifth-order-accurate upwind-biased differencing of the convective terms as an essential tool in reducing numerical diffusion and achieving reasonable agreement with measured vortex velocity profiles. Also, grid independence for Rott's analytical vortex problem was achieved using a grid spacing of $\Delta(z'/r_c) = \Delta(y'/r_c) = 0.74\Delta(x'/r_c)$ or smaller, which is equivalent to $5 \times 10^{-3}c$ or smaller. Lastly, the production term in the BB one-equation model was modified to suppress excessive numerical diffusion of the vortex caused by the turbulence model. The results showed an improvement in the prediction of the viscous vortex core over the unmodified version.

These findings were then incorporated into the full geometry case. The authors found that for a minimum grid size of 1.5 million grid points (single grid approach), the error

from numerics and the 'error' contributed by the turbulence models are of the same order of magnitude and so their separate contribution to the inaccuracy of the solution was not quantifiable. Refining the grid further (in the cross-flow plane) to obtain a total of 2.5 million grid points improve the comparisons between computation and experiment in the all three stages of development. This suggests that they were successful in reducing the numerical errors compared with turbulence modeling errors.

Addressing the numerical diffusion, which might be coming from the turbulence modeling, was not straightforward. As a preliminary attempt, an *ad-hoc* modification on the production terms of the one-equation models considered here was implemented, which gave some improvement in the resolution of the viscous vortex core. However, the fact that the principle axes of the Reynolds stress and mean strain rate tensors are not aligned suggests that an eddy viscosity approach (constant or isotropic) will most likely not be fully successful in resolving tip vortex flows. In addition, the authors showed that the resolution of the viscous vortex core properties are dependent not only on the core circumferential velocity distribution but also on the turbulent stress terms in the near-field of a wing tip. Consequently, this issue will need to be studied further.

REFERENCES

1. G.R. Srinivasan, W.J. McCroskey, J.D. Baeder and T.A. Edwards, 'Numerical simulation of tip vortices of wings in subsonic and transonic flows', *AIAA J.*, **26**, 1153–1162 (1988).
2. R. Arndt and B. Maines, 'Viscous effects in tip vortex cavitation and nucleation', *20th Symp. on Naval Hydrodynamics*, Santa Barbara, CA, August 1994.
3. J. Dacles-Mariani, S. Rogers, D. Kwak, G.G. Zilliac and J. Chow, 'A computational study of a wingtip vortex flow field', *AIAA 93-3010 AIAA Conference*, Orlando, FL, June 1993.
4. J. Dacles-Mariani, G.G. Zilliac, J. Chow and P. Bradshaw, 'A numerical/experimental study of a wingtip vortex in the near-field', *AIAA J.*, **33**, 1561–1568 (1995).
5. J. Dacles-Mariani, D. Kwak and G. Zilliac, 'Incompressible Navier–Stokes procedure for a wingtip vortex flow analysis', *6th Int. Symp. on Computational Fluid Dynamics*, Lake Tahoe, NV, September 4–8, 1995.
6. W.J. McCroskey, 'The characterization and modification of wakes from lifting vehicles in fluids', *Technical Evaluation Report*, AGARD Fluid Dynamics Panel Symposium, May, 1996.
7. J. Dacles-Mariani, D. Kwak and G. Zilliac, 'Accuracy assessment of a wingtip vortex flow field in the near-field region', *AIAA 96-0208, 34th Aerospace Sciences Meeting & Exhibit*, Reno, NV, January 15–18, 1996.
8. G. Zilliac, J. Chow, J. Dacles-Mariani and P. Bradshaw, 'Turbulent structure of a wingtip vortex in the near-field', *AIAA 24th Conference in Fluid Dynamics, AIAA 93-3011*, Orlando, FL, July 1993.
9. J. Chow, G. Zilliac and P. Bradshaw, 'Initial roll-up of a wingtip vortex in the near-field', *Proc. Aircraft Wake Vortices Conference*, vol. II, FAA, Washington DC, October 29–31, 1991, pp. 35-1–35-17.
10. J. Chow, G. Zilliac and P. Bradshaw, 'Near-field formation of a turbulent wingtip vortex', *AIAA 93-0551, AIAA Aerospace Sciences Meeting*, Reno, NV, January 11–14, 1993.
11. S. Rogers, D. Kwak and C. Kiris, 'Steady and unsteady solutions of the incompressible Navier–Stokes equations', *AIAA J.*, **29**, 603–610 (1991).
12. A. Chorin, 'A numerical method for solving incompressible viscous flow problems', *J. Comput. Phys.*, **2**, 12–26 (1967).
13. P. Roes, 'Approximate Riemann solvers, parameter vectors, and difference schemes', *J. Comput. Phys.*, **43**, 357–372 (1981).
14. N. Rott, 'On the viscous core of a line vortex', *J. Appl. Math. Phys.*, **9b**, 543–553 (1958).
15. W. Chan, I. Chiu and P. Buning, 'User's manual for the HYPGEN hyperbolic grid generator and the HGUI graphical user interface', *NASA TM 108791*, October, 1993.
16. J. Steinbrenner, J. Chawner and C. Fouts, 'The GRIDGEN 3D multiple block grid generation system', vol. II, *User's Manual, Interim Report*, October 1987–1990.
17. M. Rai, 'Navier–Stokes simulations of blade–vortex interaction using high-order-accurate upwind schemes', *AIAA Paper No. 87-0543*, Reno, NV, January 1987.
18. B. Baldwin and T. Barth, 'A one-equation transport model for high Reynolds number wall bounded flows', *NASA TM 102847*, August 1990.

19. P. Spalart and S. Allmaras, 'A one-equation turbulence model for aerodynamic flows', *AIAA Paper 92-0439*, Reno, NV, January 1992.
20. P. Spalart, *Private Communication*, Boeing Corporation, 1993.
21. W. Phillips and J. Graham, 'Reynolds stress measurement in a turbulent trailing vortex', *J. Fluid Mech.*, **147**, 353–371 (1984).